THE JOURNAL OF BIOLOGICAL CHEMISTRY VOL. 283, NO. 15, pp. 10147–10161, April 11, 2008

Structural Characterization of PTX3 Disulfide Bond Network and Its Multimeric Status in Cumulus Matrix Organization*[S]

Received for publication, October 15, 2007, and in revised form, January 24, 2008 Published, JBC Papers in Press, January 25, 2008, DOI 10.1074/jbc.M708535200

Antonio Inforzato[‡§1,2], Vincenzo Rivieccio[¶1], Antonio P. Morreale[‡], Antonio Bastone[‖], Antonietta Salustri[**], Laura Scarchilli[**], Antonio Verdoliva[¶], Silvia Vincenti[‡], Grazia Gallo[‡], Caterina Chiapparino[‡], Lucrezia Pacello[‡], Eleonora Nucera[‡], Ottaviano Serlupi-Crescenzi[‡], Anthony J. Day[§], Barbara Bottazzi[‡‡], Alberto Mantovani[‡‡], Rita De Santis[‡], and Giovanni Salvatori[‡3]

From the [‡]Sigma-Tau Research and Development, Pomezia 00040, Italy, [§]Wellcome Trust Centre for Cell-Matrix Research, Faculty of Life Sciences, University of Manchester, Manchester M13 9PT, United Kingdom, [¶]Tecnogen S.p.A., Piana di Monte Verna 81015, Italy, [‖]Istituto Ricerche Farmacologiche "Mario Negri," Milan 20157, Italy, [**]Department of Public Health and Cell Biology, University of Rome "Tor Vergata," Rome 00133, Italy, and [‡‡]Istituto Clinico Humanitas (ICH), Rozzano 20089, Italy

PTX3 is an acute phase glycoprotein that plays key roles in resistance to certain pathogens and in female fertility. PTX3 exerts its functions by interacting with a number of structurally unrelated molecules, a capacity that is likely to rely on its complex multimeric structure stabilized by interchain disulfide bonds. In this study, PAGE analyses performed under both native and denaturing conditions indicated that human recombinant PTX3 is mainly composed of covalently linked octamers. The network of disulfide bonds supporting this octameric assembly was resolved by mass spectrometry and Cys to Ser site-directed mutagenesis. Here we report that cysteine residues at positions 47, 49, and 103 in the N-terminal domain form three symmetric interchain disulfide bonds stabilizing four protein subunits in a tetrameric arrangement. Additional interchain disulfide bonds formed by the C-terminal domain cysteines Cys^{317} and Cys^{318} are responsible for linking the PTX3 tetramers into octamers. We also identified three intrachain disulfide bonds within the C-terminal domain that we used as structural constraints to build a new three-dimensional model for this domain. Previously it has been shown that PTX3 is a key component of the cumulus oophorus extracellular matrix, which forms around the oocyte prior to ovulation, because cumuli from $PTX3^{-/-}$ mice show defective matrix organization. Recombinant PTX3 is able to restore the normal phenotype *ex vivo* in cumuli from $PTX3^{-/-}$ mice. Here we demonstrate that PTX3 Cys to Ser mutants, mainly assembled into tetramers, exhibited wild type rescue activity, whereas a mutant, predominantly composed of dimers, had impaired functionality. These findings indicate that protein oligomerization is essential for PTX3 activity within the cumulus matrix and implicate PTX3 tetramers as the functional molecular units required for cumulus matrix organization and stabilization.

The long pentraxin PTX3 is an acute phase glycoprotein induced in a variety of somatic and natural immunity cells by primary inflammatory stimuli (*e.g.* Toll-like receptor engagement, interleukin-1β, tumor necrosis factor-α, and interleukin-10) (1–5). Studies performed on *Ptx3*-null ($Ptx3^{-/-}$) mice have shown that this molecule has a number of functions *in vivo*. PTX3 acts as a soluble pattern recognition receptor with a non-redundant protective role against selected pathogens, mainly the opportunistic fungus *Aspergillus fumigatus* (6, 7). PTX3 is also essential for correct assembly of the viscoelastic hyaluronan (HA)[4]-rich matrix surrounding the oocyte in the preovulatory follicle (namely, the cumulus oophorus). In fact $Ptx3^{-/-}$ mice show severe female subfertility because of defective cumulus organization (8, 9). A number of PTX3 ligands have been described so far, suggesting different physiological and/or pathological roles for this protein. PTX3 binds with high affinity to the complement component C1q thus activating the complement system through the classical pathway (10, 11). The selective recognition of fibroblast growth factor-2 (FGF-2) by PTX3 inhibits FGF-2 angiogenic activity on endothelial cells (12) and blocks the autocrine and paracrine stimulation exerted by FGF-2 on smooth muscle cells (13). Previous studies on $Ptx3^{-/-}$ mice suggested that PTX3 acts as a central "node" in cumulus matrix organization by establishing multivalent contacts to the HA-binding protein tumor necrosis factor-stimulated gene-6 protein (TSG-6) (9, 14, 15) and the serum protein inter-α-inhibitor (16). PTX3 also plays a role in regulating the scavenger activity of macrophages and dendritic cells by direct binding to apoptotic cells (17–20).

This broad binding capacity is likely to be due to the structural complexity of the protein as compared with the classical short pentraxins, C-reactive protein (CRP) and serum amyloid P component (SAP) (21). Like other members of the long pentraxin subfamily, human PTX3 is composed of a pentraxin-like

* The costs of publication of this article were defrayed in part by the payment of page charges. This article must therefore be hereby marked "*advertisement*" in accordance with 18 U.S.C. Section 1734 solely to indicate this fact.

[S] The on-line version of this article (available at http://www.jbc.org) contains supplemental Figs. S1–S3.

[1] Both authors contributed equally to this work.

[2] Supported by an international postdoctoral "Leonino Fontana and Maria Lionello" fellowship from Fondazione Italiana per la Ricerca sul Cancro (F.I.R.C.).

[3] To whom correspondence should be addressed: Immunology Area, R&D Dept., Sigma-Tau Industrie Farmaceutiche Riunite S.p.A., Via Pontina km 30.400, 00040 Pomezia, Rome, Italy. Tel.: 39-06-9139-3847; Fax: 39-06-9139-3988; E-mail: giovanni.salvatori@sigma-tau.it.

[4] The abbreviations used are: HA, hyaluronan; FGF-2, fibroblast growth factor-2; TSG-6, tumor necrosis factor-stimulated gene-6 protein; CRP, C-reactive protein; SAP, serum amyloid P component; NP2, neuronal pentraxin 2, also known as neuronal activity-regulated pentraxin (Narp); NP1, neuronal pentraxin 1; MALDI, matrix-assisted laser desorption ionization; ESI, electrospray ionization; LC, liquid chromatography; MS, mass spectrometry; CID, collision-induced dissociation; COC, cumulus cell-oocyte complex; wt, wild type; CHO, Chinese hamster ovary; DTT, dithiothreitol; WB, Western blot; TOF, time-of-flight; HPLC, high pressure liquid chromatography.

C-terminal domain (amino acids 179–381), which is homologous to the entire short pentraxin amino acid sequence, and an unrelated N-terminal region (amino acids 18–178) (22, 23). The human protein has a unique *N*-glycosylation site at Asn^{220} that has been described to be fully occupied by complex type oligosaccharides, mainly fucosylated and sialylated biantennary sugars (24). PTX3 glycosylation status affects the protein interaction with C1q thus modulating PTX3-mediated activation of the complement classical pathway (24). Studies performed with recombinant isolated forms of both PTX3 C- and N-terminal domains provided preliminary information on regions of the molecule involved in ligands recognition. The C1q-binding site appears to be localized in the C-terminal domain as expected from the known interaction of both CRP and SAP with C1q (23, 25–28). Structural determinants of the interaction with inter-α-inhibitor and FGF-2 are localized in the N-terminal domain (16, 29).

In addition to the multidomain organization, PTX3 shows a complex quaternary structure with subunits assembled into high order oligomers stabilized by disulfide bonds as demonstrated by electrophoretic and chromatographic analyses (23). Emerging evidence suggests that both short and long pentraxins express distinct bioactivities depending on subunit organization. For example, native CRP inhibits platelet activation and prevents platelet capture of neutrophils, whereas monomeric CRP, resulting from loss of the pentameric symmetry of the molecule, displays potent prothrombotic activities (30, 31). Moreover disruption of the pentameric structure, as achieved by urea treatment or by site-directed mutagenesis, leads to enhanced CRP binding to C1q and subsequent C1 activation as well as the ability of CRP to interact with complement-regulatory proteins factor H and C4b-binding protein (32). Neuronal pentraxin 2 (NP2), also known as neuronal activity-regulated pentraxin (Narp), and neuronal pentraxin 1 (NP1), two members of the long pentraxin subfamily selectively expressed in brain, are covalently linked by disulfide bonds into highly organized complexes (33, 34). The number of protein molecules in these complexes is dynamically dependent upon the activity history of the neurons and the brain developmental stage (35). However, little is known about the effect of protein oligomerization on PTX3 biological activity. It has been shown that the recombinant isolated PTX3 C-terminal domain, expressed as a monomeric species, is not able to bind C1q unless polymerized through chemical cross-linking, thus suggesting a role for the protein multimer in complement recognition possibly dependent on avidity and/or cooperativity mechanisms (23).

Short pentraxins show typical pentameric symmetry with protomer subunits held together by non-covalent interactions (21). PTX3 C-terminal domain three-dimensional structures have been elaborated by homology modeling based on human SAP (Protein Data Bank code 1sac) and CRP (Protein Data Bank code 1b09) crystal structures (22, 24, 36–38). Most interestingly, the pattern of amino acid residues located at the protomer interface in SAP pentamers is not conserved in PTX3, suggesting that PTX3 quaternary assembly might not fit the characteristic short pentraxin pentameric arrangement (38). In contrast to CRP and SAP, PTX3 oligomers are stabilized by covalent bonds (23). The mature protein contains nine cysteine residues: three are located within the N-terminal region (Cys^{47}, Cys^{49}, and Cys^{103}), and six are in the C-terminal domain (Cys^{179}, Cys^{210}, Cys^{271}, Cys^{317}, Cys^{318}, and Cys^{357}). Cys residues at positions 210 and 271 are highly conserved among pentraxins and based on the homology with CRP and SAP are predicted to be engaged in an intrachain disulfide bond (22, 23).

In this study we resolved the recombinant PTX3 oligomeric assembly, determining the number of subunits forming the functional protein. Both SDS-PAGE, performed under non-reducing conditions, and native-PAGE, carried out according to the Ferguson plot method, showed PTX3 to form mainly covalent octamers. We then identified the network of disulfide bonds stabilizing PTX3 multimers by exploiting two complementary approaches: mass spectrometry and Cys to Ser site-directed mutagenesis. Based on data from both techniques a topological map of PTX3 interchain disulfide bonds was drawn where the protein molecule is represented as a covalent octamer composed of two equivalent tetramers. The contribution of disulfide bonds to protein oligomerization was assessed by PAGE analysis under non-denaturing conditions. The new structural constraints were used to build a refined model of the PTX3 C-terminal domain.

A previous study showed that cumuli from *Ptx3*-deficient mice are unable to organize the glycosaminoglycan HA in a stable matrix and that exogenously added recombinant PTX3 rescues defective cumulus expansion *ex vivo* (9, 16). We report here that the rescue activity of PTX3 mutants, forming tetramers instead of octamers, was comparable to that of the wt protein. PTX3 mutants, lacking the entire set of interchain disulfide bonds and mainly composed of dimers, proved less effective than the wt protein in rescuing defective cumulus expansion. PTX3 oligomerization is thus essential to protein functionality within the cumulus matrix. Moreover the two tetramers composing the native PTX3 octamer appear to act as functional units in cumulus matrix organization. These findings showed that PTX3 multimeric status plays a key role in defining the biological activity of the protein.

EXPERIMENTAL PROCEDURES

Purified Proteins and Antibodies—Human recombinant PTX3 was purified from a CHO 3.5 cell line stably and constitutively expressing the protein as described previously (39). Molecular weight calibrants (thyroglobulin, ferritin, catalase, lactate dehydrogenase, and bovine serum albumin) were purchased from GE Healthcare. Biotin-labeled rabbit anti-human PTX3 polyclonal antibody αPTX3pb and rat anti-human PTX3 monoclonal antibody MNB4 were obtained from "Mario Negri" Pharmacological Research Institute, Milan, Italy. Horseradish peroxidase-conjugated streptavidin was from GE Healthcare, and rabbit anti-rat IgG-horseradish peroxidase conjugate was from Dako, Glostrup, Denmark.

Enzymes and Chemicals—Proteomics grade trypsin (from porcine pancreas), α-chymotrypsin (N^{α}-*p*-tosyl-L-lysine chloromethyl ketone-treated from bovine pancreas), endoproteinase Asp-N (from *Pseudomonas fragi* mutant strain), and endoproteinase Glu-C (from *Staphylococcus aureus* V8) were purchased from Sigma-Aldrich. DNA *Taq* polymerase and restriction enzymes applied in molecular cloning were from

Takara Bio, Otsu, Japan. Tris acetate 3–8% gradient gels were obtained from Invitrogen. Other electrophoresis reagents and nonfat dry milk were from Bio-Rad. Hybond-C Extra nitrocellulose membranes and ECL Plus Western blotting detection reagents were from GE Healthcare. Phosphate-buffered saline tablets, Tris base, NH_4HCO_3, NaCl, Tween 20, dithiothreitol (DTT), iodoacetamide, and α-cyano-4-hydroxycinnamic acid were purchased from Sigma-Aldrich. All other reagents and solvents were from Carlo Erba, Rodano, Italy and were of the highest purity available.

Ferguson Plot—Aliquots of purified recombinant PTX3 (5 μg/lane) were loaded on homogeneous polyacrylamide gels cast at 5.0, 5.5, 6.0, and 6.5% (w/v) total acrylamide concentration (% T) in the absence of SDS. Runs were performed under non-denaturing conditions in 50 mM Tris-HCl, 200 mM glycine, pH 8.3, at 150-V constant voltage for 1 h, and proteins were detected by Coomassie staining. Thyroglobulin (669 kDa), ferritin (440 kDa), catalase (232 kDa), lactate dehydrogenase (140 kDa), and bovine serum albumin (67 kDa) were used as molecular mass calibrants. Protein mobility was analyzed by Ferguson plot as described previously (40). Briefly the relationship between protein mobility (μ) and sieving matrix concentration (% T) may be written as

$$\log_{10}(\mu) = \log_{10}(\mu_0) - K_r(\%\,T) \qquad \text{(Eq. 1)}$$

where μ_0 is the free solution mobility (zero concentration of sieving matrix) and K_r is the retardation coefficient (which is directly related to protein shape and molecular weight). A standard curve (namely the Ferguson plot) was constructed by plotting the logarithm of calibrant relative mobility ($\log_{10}R_f$) as a function of total polyacrylamide concentration (% T). Retardation coefficients (K_r) were then computed from the plot slope and graphed *versus* molecular mass (K_r plot). PTX3 samples were processed in the same way as the calibrants, and their molecular mass was finally calculated by K_r plot interpolation.

In a separate set of experiments, electrophoresis mobility data for Ferguson plot analysis of purified recombinant PTX3 were derived from Western blots (WBs). Briefly aliquots of protein (20 ng/lane) were loaded on native gels and run under the same experimental conditions as above. Gels were then blotted onto nitrocellulose membranes, revealed by immunodetection (see below), and submitted to Ferguson plot analysis as described above.

SDS-PAGE and WB—Aliquots of purified recombinant PTX3 (either 2 μg for Coomassie staining or 20 ng for immunodetection) were resolved on Tris acetate 3–8% gradient or Tris-glycine 9% homogeneous gels under denaturing conditions in the presence or absence of DTT. Following electrophoresis, proteins were either revealed by Coomassie staining or transferred to Hybond-C Extra nitrocellulose membranes for subsequent immunodetection. Blotted membranes were blocked with 5% nonfat dry milk in Tris-buffered saline containing 0.05% (v/v) Tween 20 (blocking buffer) for 2 h at room temperature and then incubated overnight at 4 °C with a 1:2,000 MNB4 dilution in blocking buffer. This antibody recognizes a linear epitope mapping in the N-terminal domain of human PTX3 (29). Following an additional incubation with rabbit anti-rat IgG-horseradish peroxidase conjugate, membranes were finally developed with ECL Plus according to the manufacturer's instructions.

PTX3 Proteolysis and MALDI-MS—Purified recombinant PTX3 in phosphate-buffered saline (1 mg/ml) was dialyzed against 100 mM NH_4HCO_3, pH 7.8, by ultrafiltration on Microcon YM-30 centrifugal filter units (Millipore, Billerica, MA). Protein samples (200 μg) were subjected to proteolysis by incubation with trypsin, α-chymotrypsin, Asp-N, or Glu-C endoproteinases. Digestions were performed in 100 mM NH_4HCO_3, pH 7.8, at 37 °C for 16 h in a 225-μl final volume using enzyme: protein ratios of 1:50, 1:100, 1:50, and 1:40 (w/w), respectively. Reactions were terminated by addition of 25 μl of 2% (v/v) trifluoroacetic acid and lyophilization. PTX3 peptide mixtures were then resuspended in 100 mM NH_4HCO_3, pH 7.8, and split in 50-μg aliquots. Some aliquots were directly submitted to MS analysis; others were first reduced and/or alkylated by incubation with 1 mM DTT for 1 h at 37 °C and/or 20 mM iodoacetamide for an additional 30 min at room temperature.

Prior to MALDI-MS analysis, peptide mixtures from endoproteinase digestions were desalted by reversed phase chromatography on an Agilent 1200 HPLC system (Agilent Technologies, Santa Clara, CA). Briefly peptide samples were loaded on a Phenomenex Jupiter C_{18} column (500 μm; 2.0-mm inner diameter × 15-cm length; particle size, 300 Å; Phenomenex, Torrance, CA) equilibrated by a 95% solvent A, 5% solvent B mixture (solvent A: 0.1% (v/v) trifluoroacetic acid; solvent B: 95% (v/v) acetonitrile, 0.1% (v/v) trifluoroacetic acid). Following an isocratic washing step at 5% solvent B for 10 min, a fast linear gradient was applied from 5 to 95% solvent B over 1 min, and peptide mixtures were eluted at 95% solvent B. The flow rate was set to 0.2 ml/min, and peptide elution was monitored as UV absorbance at both 216 and 280 nm. Peptide mixtures, eluted as a single peak, were manually collected and immediately freeze-dried. Positive ion MALDI-MS analyses of PTX3 peptides were carried out on a Bruker Daltonics Reflex II TOF/TOF MALDI spectrometer (Bruker Daltonics, Billerica, MA) operating in reflectron mode. The MALDI matrix was prepared by dissolving 10 mg of α-cyano-4-hydroxycinnamic acid in 1 ml of acetonitrile, 0.2% (v/v) trifluoroacetic acid (70:30, v/v). Typically 1 μl of matrix was applied to the metallic sample plate, and 1 μl of analyte was then added. Acceleration and reflector voltages were set as follows: target voltage at 20 kV, first grid at 95% of target voltage, and delayed extraction at 200 ns. Raw data were analyzed using computer software provided by the manufacturer and are reported as monoisotopic masses.

LC/ESI-MS/MS—PTX3 peptides from protease digestions were also analyzed on a SpectraSystem HPLC system (Thermo Fisher Scientific, Waltham, MA) equipped with a P6000 pump and a UV6000LP UV-visible detector connected to the ESI probe of an LCQ Duo ion trap mass spectrometer (ThermoFinnigan, San Jose, CA). Peptide samples were loaded on a Supelco Discovery® BIO wide pore C_{18} column (500 μm; 2.1-mm inner diameter × 15-cm length; particle size, 300 Å; Sigma-Aldrich) equilibrated by a 97% solvent A, 3% solvent B mixture. A linear gradient was then developed from 3 to 58% solvent B over 55 min. Tryptic mixtures were chromatographed on a shallower linear gradient ramping from 3 to 58% solvent B

TABLE 1
Primers used to generate PTX3 Cys to Ser mutants by overlapping PCR

Primers	Primer sequences[a]	Cloning enzymes[b] (fragment length in bp)
C47S		
Sense 1	5′-TGTCCCTTGTATCACCATGGACCCTCA-3′	MfeI-SapI (576)
Antisense 1	5′-GCAGTC**GGA**CGGCGTGGG-3′	
Sense 2	5′-G**TCC**GACTGCGGTCAGGAGCA-3′	
Antisense 2	5′-TGCAGGATTCCTCCCTCAGGAACAA-3′	
C49S		
Sense 1	5′-TGTCCCTTGTATCACCATGGACCCTCA-3′	MfeI-SapI (576)
Antisense 1	5′-**GGA**GTCGCACGGCGTGGG-3′	
Sense 2	5′-GTGCGAC**TCC**GGTCAGGAGCA-3′	
Antisense 2	5′-TGCAGGATTCCTCCCTCAGGAACAA-3′	
C103S		
Sense 1	5′-GGGACAAGCTCTTCATCATGCTGGAGAA-3′	SapI-Bsu36I (764)
Antisense 1	5′-C**GGA**CGGCCTCGCCAGGCTTT-3′	
Sense 2	5′-AAAGCCTGGCGAGGCCG**TCC**G-3′	
Antisense 2	5′-AATCTGCAGGATTCCTCCCTCAGGAACA-3′	
C317S/C318S		
Sense 1	5′-CCTGGCCGCGGTGCTAGAGGA-3′	SacI-SacII (701)
Antisense 1	5′-ACCACCCAC**AGAGGA**GCCATTCTTTTCTTG-3′	
Sense 2	5′-CAAGAAAAGAATGGC**TCCTCT**GTGGGTGGT-3′	
Antisense 2	5′-ATGAAACATACTGAGCTCCTCCATGTGGCT-3′	

[a] Serine codons are bold. Mutated bases are underlined.
[b] Enzymes used to clone overlapping PCR products into the pSG5hPTX3 backbone.

over 80 min. In both cases, the flow rate was set to 0.2 ml/min followed by a splitting ratio of ~1:20. Peptide elution was monitored as both UV absorbance at 216 and 280 nm and total ion current. A spray voltage of 4.5 kV, capillary temperature of 280 °C, capillary voltage of 39 V, and tube lens offset of 10 V were used. A triple play (full scan, ZoomScan, and CID with 30–40% collisional energy) data-dependent acquisition method with dynamic exclusion was performed using the Xcalibur software (ThermoFinnigan). Spectra were processed using the base peak ion chromatogram and a seven-point Gaussian smoothing function.

Cys to Ser PTX3 Mutant Constructs—C47S, C49S, C103S, C47S/C49S, and C317S/C318S mutant constructs were produced where cysteine codons at amino acid positions 47, 49, 103, 47/49, and 317/318 were replaced with serine-coding triplets. Site-directed mutagenesis was performed by overlapping PCR (41). The plasmid vector pSG5 (Stratagene, La Jolla, CA) containing the full-length human *PTX3* cDNA sequence (pSG5hPTX3) was used as a template (39). Overlapping primers (see Table 1) were designed using Oligo software (version 6.71) and synthesized by MWG-Biotech, Milan, Italy. DNA amplifications were performed in a total volume of 100 μl including 500–1000 ng of DNA template, 0.2 μM primers, 0.25 mM dNTPs, 10 units of *Taq* polymerase, 1.5 mM $MgCl_2$, and 2× GC buffer 1 (Takara Bio). Following an initial denaturation step at 95 °C for 5 min, 25–30 thermal cycles were set as follows: 30–60-s denaturation at 95 °C, 30–60-s annealing at the optimal annealing temperature of the primers (62–72 °C), and 45–60-s elongation at 72 °C. A final extension step was applied at 72 °C for 5 min. PCR products were then purified on agarose gels and overlapped by PCR under the same experimental conditions described above. Overlapped fragments were again purified on agarose gels, digested with the appropriate restriction enzymes (see Table 1), and finally cloned into an empty pSG5hPTX3 vector. C47S/C49S/C103S and C47S/C49S/C103S/C317S/C318S mutant constructs, containing Cys to Ser mutations at amino acid positions 47/49/103 and 47/49/103/317/318, respectively, were produced by sequential subcloning. Precisely C47S/C49S/C103S was generated by subcloning the $pSG5hPTX3Cys_{103}$ insert into the $pSG5hPTX3Cys_{47/49}$ vector through SapI and SacII endonuclease restriction, and C47S/C49S/C103S/C317S/C318S was generated by subcloning the $pSG5hPTX3Cys_{317/318}$ insert into the $pSG5hPTX3Cys_{47/49/103}$ vector through SacI and SacII restriction. These constructs were then expressed in CHO cell lines as described below.

Cell Culture and Protein Expression—CHO cells (BD Biosciences) were transiently transfected with uncleaved plasmid DNA using Lipofectamine reagent (Invitrogen). Following transformation, cells were incubated for 48 h in serum-free medium (Dulbecco's modified Eagle's medium, Sigma-Aldrich) in a humidified incubator gassed with 5% CO_2, 95% air at 37 °C. Cell culture supernatants were then collected by centrifugation at 1,500 rpm for 10 min and stored at −80 °C. The protein concentration in culture supernatants was measured by a sandwich enzyme-linked immunosorbent assay based on the monoclonal antibody MNB4 and the rabbit polyclonal antibody αPTX3pb as reported previously (5, 24). Supernatant aliquots containing 20 ng of proteins were analyzed by WB under both denaturing and non-denaturing conditions as described above. Protein bands were quantitated by densitometry analysis using Eastman Kodak Co. Gel Logic 100 software. Electrophoretic mobilities from native WB were finally used to draw Ferguson and K_r plots.

Aliquots of culture supernatants from CHO cells transfected with C47S/C49S/C103S, C317S/C318S, and C47S/C49S/C103S/C317S/C318S mutant constructs were submitted to a chromatographic purification. Briefly following a 10-fold concentration step on 100-kDa-cutoff Pellicon-Biomax 100 ultrafiltration membranes (Millipore), supernatant aliquots were loaded onto a 100-ml Q-Sepharose™ Fast Flow (GE Healthcare) packed column (5 × 51 mm). The column was equilibrated previously with 50 mM Tris-HCl, 0.3 M NaCl, pH 7.00, at a linear flow rate of 76 cm/h, and the effluent was monitored by UV detection at 280 nm. Retained material was eluted using a

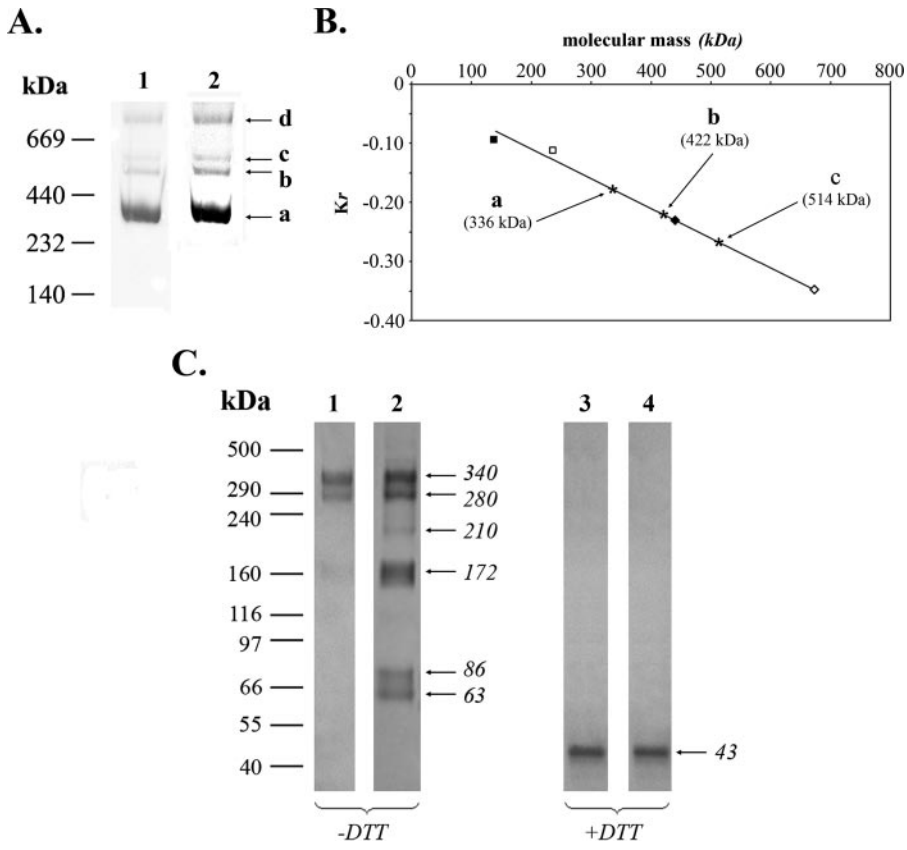

FIGURE 1. **PTX3 molecular weight determination.** *A*, purified recombinant PTX3 aliquots were loaded on homogeneous polyacrylamide gels cast at 5.0, 5.5, 6.0, and 6.5% T and run under non-denaturing conditions. Only a 5.5% gel is shown as representative of the observed electrophoretic profiles. Proteins were either Coomassie-stained (*lane 1*) or blotted onto nitrocellulose filters and detected by rat α-human PTX3 monoclonal antibody MNB4 (*lane 2*). The molecular masses of thyroglobulin (669 kDa), ferritin (440 kDa), catalase (232 kDa), and lactate dehydrogenase (140 kDa) were used as calibrants. The positions of bands a, b, c, and d are indicated by *arrows*. *B*, retardation coefficients (K_r) computed from calibrant Ferguson plots (see "Experimental Procedures") were graphed *versus* molecular mass (K_r plot) and used to determine the molecular mass of bands a, b, and c. The position of the calibrants is indicated. (◇, thyroglobulin; ◆, ferritin; □, catalase; ■, lactate dehydrogenase.). *C*, purified recombinant PTX3 was resolved on Tris acetate 3–8% gradient gels under denaturing conditions in the absence (−*DTT*) or presence (+*DTT*) of dithiothreitol. Gels were either Coomassie-stained (*lanes 1* and *3*) or blotted onto nitrocellulose filters and detected as in *A* (*lanes 2* and *4*). Apparent molecular mass of the resolved bands is shown.

nonlinear gradient, raising the mobile phase conductivity stepwise to 42 millisiemens/cm to wash the resin and then to 60 millisiemens/cm to elute PTX3. PTX3-containing fractions (eluted at 60 millisiemens/cm) were quantitated by enzyme-linked immunosorbent assay as described above and then applied to cumulus cell-oocyte complex (COC) culture and hyaluronan labeling experiments (see below).

Structure Prediction—The MacroModel molecular mechanics package (42) was used to generate a PTX3 C-terminal domain three-dimensional model based on the x-ray structure of CRP (Protein Data Bank code 1b09) with which it has 26.8% identity (42.7% similarity). Intrachain disulfide bonds revealed by mass spectrometry and site-directed mutagenesis were integrated into the model, and structure optimization was performed by molecular dynamics (optimized potential for liquid simulation-all atom force field in water, 200 ps at 300 K, using a 300 kJ $mol^{-1}Å^{-2}$ constraint on β-strand and α-helical motives). Twenty structures were extracted and minimized using steepest descent and truncated Newton conjugate gradient algorithms up to a convergence criterion of 5×10^{-3} kJ mol^{-1} $Å^{-1}$. The best solution in terms of percentage of amino acids in the most favored and allowed regions (Ramachandran plots) was chosen using the utility Procheck (43).

COC Culture and Hyaluronan Labeling—Adult Sv129 wild type and *Ptx3*-deficient mice (8) were injected with 5 IU of pregnant mare serum gonadotrophin, and ovaries were collected 48 h later. COCs were isolated and cultured for 16 h at 37 °C in 5% CO_2 under a 20-μl oil drop in modified Eagle's medium (Sigma-Aldrich) supplemented with 3 mM glutamine, 0.3 mM sodium pyruvate, and 50 ng/ml gentamycin in the presence of 100 ng/ml follicle-stimulating hormone, 1% fetal bovine serum, [^{35}S]sulfate (60 μCi/ml), and [^{3}H]glucosamine (100 μCi/ml) (PerkinElmer Life Sciences). At the start of the cultures, wild type recombinant PTX3 or PTX3 mutants were added to $Ptx3^{-/-}$ COCs at the concentrations indicated in the text. Medium and cell matrix were collected separately, and the amount of HA in the two compartments was determined as described elsewhere (9).

RESULTS

PTX3 Molecular Weight Determination—PTX3 is a multimeric glycoprotein composed of identical subunits held together by interprotomer disulfide bonds (23). The number of protomers forming the functional molecule has not yet been clearly defined. To address this point we measured PTX3 molecular weight by PAGE under both native and denaturing conditions. Samples of human recombinant PTX3 expressed in CHO cells were applied onto polyacrylamide continuous gels cast at four different acrylamide concentrations (5.0, 5.5, 6.0, and 6.5% T) and resolved under native conditions. Fig. 1*A* shows the 5.5% gel as representative of the observed electrophoretic profiles. By Coomassie staining (*lane 1*) a characteristic pattern was revealed with one major band (a) running between catalase (232 kDa) and ferritin (440 kDa), two minor bands (b and c) migrating between ferritin and thyroglobulin (669 kDa), and an additional signal above thyroglobulin standard (d). An identical profile was observed following gel blotting onto a nitrocellulose filter and PTX3 detection by monoclonal antibody MNB4 (*lane 2*), thus confirming that the species revealed by Coomassie staining were indeed PTX3 oligomers. Data from native gels were then submitted to Ferguson plot analysis (40). Log_{10} relative mobility ($log_{10}R_f$) was plotted *versus* gel concentration (% T) for

both PTX3 and protein standards. Retardation coefficients (K_r) were computed from the slope of the respective plots and graphed *versus* molecular mass (K_r plot). Finally the molecular mass of bands a, b, and c was calculated by K_r plot interpolation and shown to be 336, 422, and 514 kDa, respectively (Fig. 1*B*). In a previous work, we characterized the recombinant human PTX3 glycosidic moiety and showed it to be mainly composed of monofucosylated disialylated biantennary complex type sugars with minor monofucosylated triantennary and tetra-antennary structures exhibiting different degrees of sialylation (24). According to this analysis, the PTX3 glycosidic moiety accounts for a contribution to the protein monomer molecular mass of about 2.5 kDa. As PTX3 polypeptide backbone has an average molecular mass of 40.165 Da (calculated from the coding DNA sequence), we assumed for the protein subunits an average molecular mass of 42.5 kDa. On the basis of this assumption, the major band (a) could be concluded to correspond to protein octamers (336/42.5 kDa, ~8), whereas the minor bands (b and c) originated from PTX3 decamers (422/42.5 kDa, ~10) and dodecamers (514/42.5 kDa, ~12), respectively. We estimated for band d a molecular mass of about 700 kDa, which is close to the molecular mass expected for PTX3 16-mers (680 kDa). However, it should be pointed out that this value is only approximate as the corresponding K_r value was outside of the K_r plot linearity range.

SDS-PAGE analysis, performed on Tris acetate 3–8% gradient gels under non-reducing conditions (Fig. 1*C*, *lane 1*), revealed a major band with an apparent molecular mass of 340 kDa, consistent with PTX3 protomers being mainly assembled into octamers and furthermore indicating that protein octamers are likely to be stabilized by disulfide bonds. No signals were detected at higher molecular weight, suggesting that bands b, c, and d from native gels correspond to PTX3 higher order oligomers held together through non-covalent interactions. A minor band was observed at 280 kDa, about 6.6 times the PTX3 protomer mass. This band probably originates from not fully denatured PTX3 octamers and/or heptamers, which retain some secondary structure and, as a consequence, show an aberrant high electrophoretic mobility. After blotting and antibody detection, several additional bands were seen at 210, 172, and 86 kDa that are likely to correspond to PTX3 pentamers, tetramers, and dimers, respectively (Fig. 1*C*, *lane 2*). The species with an apparent molecular mass of 63 kDa may correspond to fast migrating protein dimers, which retain some secondary structure, as suggested above for the signal at 280 kDa. Upon reduction, only one band at 43 kDa (close to the expected molecular mass for PTX3 monomers) was observed following either Coomassie staining (Fig. 1*C*, *lane 3*) or Western blotting (Fig. 1*C*, *lane 4*), indicating that the high molecular weight species detected under non-reducing conditions are indeed PTX3 homo-oligomers and do not contain any other protein.

Mass Spectrometry—As described above, electrophoresis analyses performed under both native and denaturing conditions revealed that recombinant human PTX3 is secreted as a mixture of oligomers the most abundant of which are likely to be covalent octamers. To characterize the network of disulfide bonds stabilizing the protein octameric assembly, PTX3 samples were subjected to proteolysis by incubation with sequence-specific endoproteinases (trypsin, Glu-C, Asp-N, and α-chymotrypsin), and the resulting peptide mixtures were analyzed by both MALDI-MS and LC/ESI-MS/MS both in presence and in absence of reducing agents.

Peptides were assigned to the PTX3 amino acid sequence on the basis of measured molecular masses and enzyme specificity. To verify sequence assignments, pseudomolecular cations of relevant peptides were selected as precursor ions and submitted to CID MS/MS experiments performed in the on-line LC/ESI-MS/MS mode. As shown in Fig. 2, assigned peptides covered 94.2% of the mature PTX3 amino acid sequence. *PTX3* encodes nine cysteines: three in the N-terminal region and six in the C-terminal pentraxin domain (23). Fragments were detected containing every cysteine apart from Cys^{47} probably because peptides containing Cys^{47} have low ionization efficiency and/or low solubility under the LC conditions exploited. No peptide was detected covering Asn^{220} when endoproteinase incubations were performed on glycosylated PTX3. As stated above, we recently described Asn^{220} as a unique *N*-glycosylation site in PTX3 and showed this site to be fully occupied in the mature secreted protein (24). PTX3 deglycosylation by peptide-*N*-glycosidase F treatment, in fact, enabled detection of additional peptides spanning Asn^{220} thus bringing sequence coverage to 96.2%.

A list of the observed cysteine-containing peptides is reported in Table 2. MS analyses performed on Asp-N digests under both reducing and non-reducing conditions demonstrated Cys^{49} to be involved in interprotomer disulfide bonds, *i.e.* pairs of PTX3 subunits are linked together through Cys^{49}-Cys^{49} bonds (Table 2 and supplemental Fig. S1). We consistently observed homodimeric peptides spanning Cys^{103}, which showed that Cys^{103} also forms interprotomer disulfide bonds (Table 2 and Fig. 3*A*). From these data it is not possible to establish whether Cys^{103} connects PTX3 subunits already cross-linked by Cys^{49} or other subunits.

Two covalent bonds were described bridging Cys^{210} to Cys^{271} (Table 2 and Fig. 3) and Cys^{179} to Cys^{357} (Table 2 and supplemental Fig. S2). These could not be unambiguously sorted into either inter- or intrachain disulfide bonds. However, it has to be noted that Cys^{210} and Cys^{271} are highly conserved among members of the pentraxins family, and these residues have been described to establish an intrachain disulfide bond essential for pentraxin fold stabilization (22, 23). Thus, it is likely that also in PTX3 Cys^{210} and Cys^{271} form intrasubunit linkages. Moreover Cys^{179} and Cys^{357} are conserved among the long neuronal pentraxins Narp and NP1 (33, 34). Some recent evidence showed that corresponding residues in these proteins do not participate in the formation of multimers (35), strongly suggesting that the disulfide bond Cys^{179}-Cys^{357} described here is formed within rather than between PTX3 subunits.

MS analysis of trypsin and Glu-C digests provided information on the redox state of cysteines 317 and 318 (Table 2). As representative of the obtained results, MALDI and CID ESI-MS/MS spectra of PTX3 tryptic mixtures are shown in Fig. 3. MALDI analysis performed under non-reducing conditions revealed a signal at 3574.48 Da (Fig. 3*A*, *upper panel* and *inset* on the *right*) that was attributed to the homodimeric peptide (315–332)-(315–332) where Cys^{317} and Cys^{318} were both

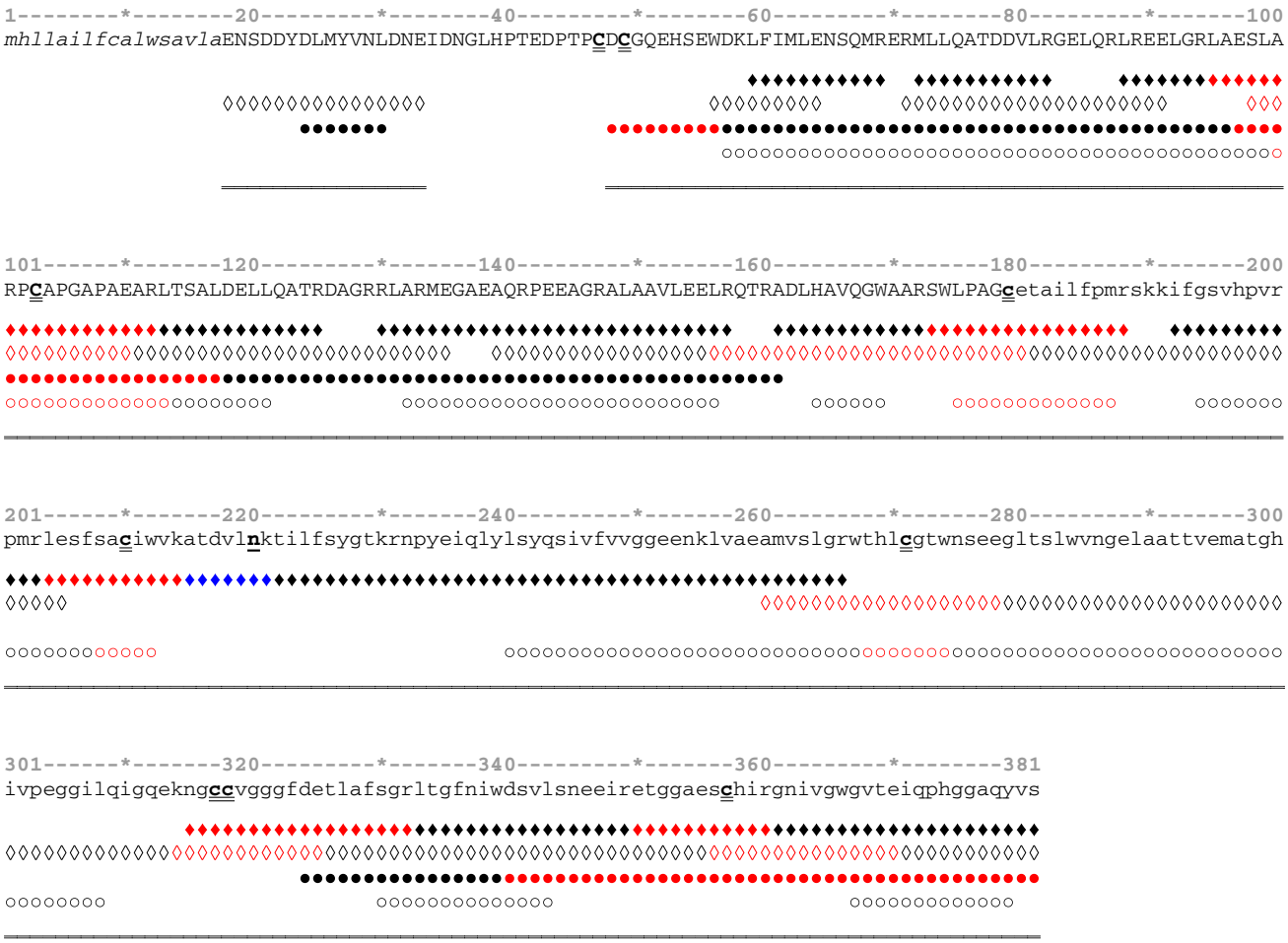

FIGURE 2. **Human PTX3 amino acid sequence and its coverage by endoproteinase digestions.** The human PTX3 amino acid sequence is reported in one-letter code. Regions covered through peptides released by trypsin (♦), endoproteinase Glu-C (◊), endoproteinase Asp-N (●), and chymotrypsin (○) digestions and identified by MS analysis are indicated. Overall coverage from the four enzymatic digestions is indicated by *double lined* sequence (=). The leader peptide is reported in *lowercase italic*. N- and C-terminal domain sequences are indicated in *capital* and *lowercase letters*, respectively. Cysteine residues (C or c) and the unique glycosylation site (n) are also shown. Cysteine-containing peptides are highlighted in *red*. Additional peptides released by endoproteinase digestions following peptide-*N*-glycosidase F treatment are highlighted in *blue*. *Asterisks* indicate middle amino acid positions between those indicated by *numbers*.

involved in disulfide bond formation (theoretical monoisotopic molecular mass of 3574.53 Da). Signal assignment was verified by MALDI analysis of DTT-reduced tryptic digests. Following reduction, in fact, the peak at 3574.48 Da disappeared (Fig. 3*A*, *lower panel* and *inset* on the *right*), whereas a new peak was detected at 1789.79 Da (Fig. 3*A*, *lower panel* and *inset* on the *left*), matching the theoretical monoisotopic molecular mass of peptide 315–332 in its reduced form (namely 1789.76 Da). We could not establish by MS/MS whether the two bonds were symmetrical (Cys^{317}-Cys^{317} and Cys^{318}-Cys^{318}) or asymmetrical (Cys^{317}-Cys^{318} and Cys^{318}-Cys^{317}) as fragmentation of the dimeric peptide (315–332)-(315–332) or the corresponding species observed in Glu-C digests (see Table 2) preferentially occurred at the disulfide bonds. It is worth noting that no free sulfhydryls were detected in the recombinant PTX3 by 5,5′-dithiobis(nitrobenzoic acid) assay (see below), so the occurrence of (315–332)-(315–332) peptides with one cysteine engaged in a disulfide bond and the other free is very unlikely. Moreover MALDI MS analysis performed under non-reducing conditions showed a signal at 1787.79 Da (Fig. 3*A*, *upper panel* and *inset* on the *left*). As this value is 2 Da less than the value calculated for peptide 315–332, it likely originates from peptide 315–332 upon formation of an interchain disulfide bond that causes the loss of two protons. Consistent with this view, DTT reduction induced a 2-Da mass shift (1789.79 Da) where the original peak at 1787.79 Da disappeared (Fig. 3*A*, *lower panel* and *inset* on the *left*). Taken together, these data showed a dual role for Cys^{317} and Cys^{318} as they are capable of forming both inter- and intrachain disulfide bonds.

To confirm the identity of species at 1787.79 and 1789.79 Da, 30% collisional energy CID experiments were performed in the on-line LC/ESI-MS/MS mode. Pseudomolecular cations at m/z 1787.73 and 1789.82 Da were selected as precursor ions, and the resulting CID spectra are shown in Fig. 3*B*. In both spectra, the most intense ion signals were y_{17} fragments due to the loss of the N-terminal Asn^{315} and y_7 and y_8 fragments arising from peptide bond fragmentation C-terminal to Asp^{324} and Glu^{325}. The observed fragmentation patterns were consistent with the sequence of peptide 315–332. Moreover identical mass values were measured for y_7 and y_8 fragments in both spectra. Because y_7 and y_8 ions both retained the peptide C-terminal end lacking cysteines 317 and 318, their observed molecular masses were

TABLE 2
PTX3 cysteine-containing peptides as released by endoproteinase digestions and identified by MS

Enzyme	Reducing conditions			Non-reducing conditions		
	Peptides	Observed molecular weight[a]	Theoretical molecular weight[a]	Peptides	Observed molecular weight[a]	Theoretical molecular weight[a]
Cys[49]						
Trypsin[b]						
Glu-C						
Asp-N	48–56	1090.43	1090.38	(48–56)–(48–56)	2178.08	2177.76
Chymotrypsin						
Cys[103]						
Trypsin[b]	95–112	1779.93	1779.92	(95–112)–(95–112)	3556.72	3556.83
Glu-C	98–110	1239.60	1239.62	(98–110)–(98–110)	2476.15	2476.23
Asp-N	97–117[c]	2081.03	2081.07	(97–117)–(97–117)	4159.23	4159.15
Chymotrypsin	100–113	1379.68	1379.71	(100–113)–(100–113)	2756.52	2756.43
Cys[179]						
Trypsin[b]	173–188	1791.91	1791.89	(173–188)–(350–360)	2948.35	2948.41
Glu-C	156–180	2792.35	2792.41	(156–180)–(356–370)	4417.09	4417.21
Asp-N						
Chymotrypsin	175–187	1362.70	1362.67			
Cys[210]						
Trypsin[b]	204–214	1282.67	1282.65			
Glu-C						
Asp-N						
Chymotrypsin	208–212	579.12	579.25	(208–212)–(268–274)	1393.70	1393.61
Cys[271]						
Trypsin[b]						
Glu-C	260–278	2176.95	2176.99			
Asp-N						
Chymotrypsin	268–274	817.29	817.36	(208–212)–(268–274)	1393.70	1393.61
Cys[317/318]						
Trypsin[b]	315–332	1789.79	1789.76	315–332	1787.80	1787.76
				(315–332)–(315–332)	3574.48	3574.53
Glu-C	314–325	1185.43	1185.47	314–325	1183.43	1183.47
				(314–325)–(314–325)	2365.79	2365.93
Asp-N						
Chymotrypsin						
Cys[357]						
Trypsin[b]	350–360	1159.50	1159.52	(173–188)–(350–360)	2948.35	2948.41
Glu-C	356–370	1627.73	1627.80	(156–180)–(356–370)	4417.09	4417.21
Asp-N	340–381	4451.89	4452.12			
Chymotrypsin						

[a] Observed and theoretical molecular weights are expressed as monoisotopic masses.
[b] MALDI-MS-measured molecular weights of tryptic peptides are reported. Molecular weights of peptides from other enzyme digests are shown as measured by ESI-MS.
[c] Peptide 97–117 comes from unspecific cleavage of the peptide bond N-terminal to Glu[97].

not affected by DTT treatment. Upon reduction, the y_{17} fragment containing the two cysteine residues underwent a 2-Da mass increase instead as previously described for the precursor ions. Finally iodoacetamide proved effective at alkylating both cysteines only after reduction by DTT (data not shown), thus confirming the covalent bond bridging Cys[317] to Cys[318].

In summary, Cys[49] and Cys[103] were shown to form interchain homologous disulfide bonds. We described cysteine residues at positions 179, 210, 271, and 357 as involved in heterologous disulfide bonds. Cys[317] and Cys[318] were found to form both inter- and intrasubunit linkages. As noted above, we attempted to measure the number of free sulfhydryls in the recombinant PTX3 by 5,5′-dithiobis(nitrobenzoic acid) assay (44, 45) where human CRP and recombinant human FGF-2 were used as negative and positive controls, respectively. However, we could not find any free sulfhydryl in PTX3 (data not shown). These measurements were able to detect free cysteines at a concentration of 2–3 μM. As we used 100 μM protein solutions, we could have detected up to nine sulfhydryls per PTX3 subunit, but we did not observe any. These findings indicate that PTX3 cysteines are all engaged in disulfide bonds and, indirectly, suggest that also Cys[47] forms a covalent linkage. Given the picture of the PTX3 disulfide bond network determined above, we must conclude that Cys[47] forms interchain homologous disulfide bridges.

Site-directed Mutagenesis—Mass spectrometry identified PTX3 cysteine residues engaged in disulfide bonds. To understand how these bonds are distributed within the subunits forming protein oligomers, *PTX3* cDNA sequence was subjected to site-directed mutagenesis. Cysteine codons at amino acid positions 47, 49, 103, 317, and 318 were replaced with serine codons to give both single and multiple Cys to Ser PTX3 mutant constructs combined as follows: C47S, C49S, C103S, C47S/C49S, C47S/C49S/C103S, C317S/C318S, and C47S/C49S/C103S/C317S/C318S. The cDNA constructs were then used to transiently transfect CHO cells. Mutant proteins, expressed as secretion products into cell culture supernatants, were quantitated by enzyme-linked immunosorbent assay and finally analyzed by Western blot under non-reducing conditions. Supernatants from wt cDNA- and mock-transfected cells were used as positive and negative controls, respectively.

wt PTX3 showed bands at 340, 280, 210, 172, 86, and 63 kDa as described for the purified protein (Fig. 4*A*, *upper panel*, as compared with Fig. 1*C*, *lane 2*), thus demonstrating that PTX3 expression was effective under the applied transfection conditions. Mock-transfected cells did not produce any PTX3 as

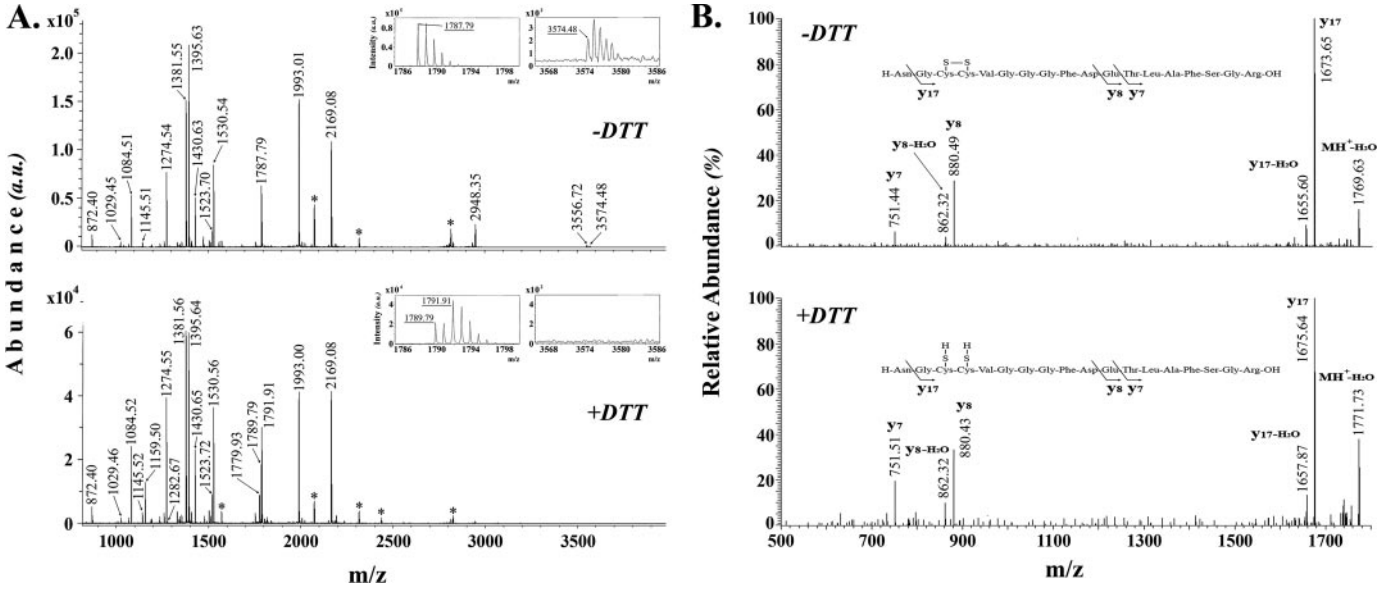

FIGURE 3. **Analysis of PTX3 tryptic digests by MALDI-MS and ESI/CID-MS/MS.** *A*, peptide mixtures from PTX3 tryptic digests were analyzed by MALDI-MS in reflectron positive ion mode. Mass spectra acquired from non-reduced (−*DTT*) and reduced (+*DTT*) mixtures are shown. *Inset panels* show expanded views of spectra spanning the molecular mass of peptide 315–332 (*left panels*) and its dimeric form (*right panels*) (see Table 2). Reported molecular mass values are expressed as monoisotopic mass. *Asterisks* refer to contaminants. *B*, non-reduced (−*DTT*) and reduced (+*DTT*) PTX3 tryptic digests were resolved by reversed phase HPLC and revealed by ESI/ion trap MS/MS. Pseudomolecular $[MH]^+$ cations at *m/z* 1787.73 and 1789.82, detected in non-reduced and reduced samples, respectively, were selected as precursor ions and submitted to CID fragmentation with 30% collisional energy. Peaks in both spectra are labeled with y ions based on mass matches to predicted fragments. Ladder diagrams with y ion numbering are shown. *a.u.*, absorbance unit.

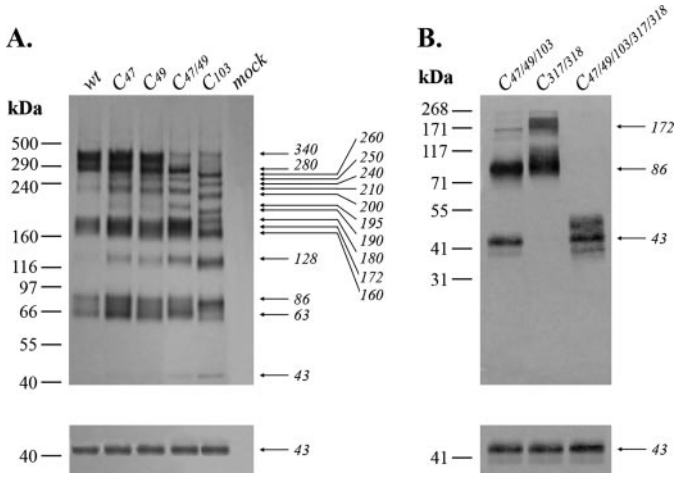

FIGURE 4. **WB analysis of PTX3 Cys to Ser mutants under denaturing conditions.** Supernatants from CHO cell cultures expressing Cys to Ser PTX3 mutants (see text) and wt PTX3 were run on 3–8% gradient (*A*) or 9% homogeneous (*B*) acrylamide gels under denaturing conditions in the absence (*upper panels*) or presence (*lower panels*) of dithiothreitol. Gels were blotted onto nitrocellulose membranes, and proteins were revealed by immunodetection with rat α-human PTX3 monoclonal antibody MNB4. Supernatants from mock-transfected cells were used as negative controls. Molecular mass markers are shown on the *left*. Apparent molecular mass values seen for the resolved bands are reported on the *right*. C47S, C49S, C47S/C49S, C103S, C47S/C49S/C103S, C317S/C318S, and C47S/C49S/C103S/C317S/C318S mutants are indicated as C_{47}, C_{49}, $C_{47/49}$, C_{103}, $C_{47/49/103}$, $C_{317/318}$, and $C_{47/49/103/317/318}$, respectively.

expected. C47S and C49S mutants exhibited electrophoresis profiles (Fig. 4*A*, *upper panel*) very similar to those observed for wt PTX3. However, an additional band at 128 kDa was detected that likely corresponds to PTX3 trimers (128/42.5 kDa, ~3). Two more bands were observed at 250 and 195 kDa, the former probably originating from PTX3 hexamers (250/42.5 kDa, ~6). Finally the signal at 210 kDa appeared more prominent as compared with that described for wt PTX3. The close similarity of the band patterns for C47S and C49S to that of the wt PTX3 indicates that Cys^{47} and Cys^{49} exert a redundant role in PTX3 covalent oligomerization. Cys^{49} was shown by MS to form interchain symmetric disulfide bonds. From the overall analysis of our MS data, we concluded that also Cys^{47} establishes interchain symmetric disulfide bridges (see above). Site-directed mutagenesis results shown here are consistent with this and furthermore suggest that Cys^{47}-Cy^{47} and Cys^{49}-Cys^{49} disulfide bonds occur within the same pairs of PTX3 subunits. As can be seen from Fig. 4, the double mutant C47S/C49S had greatly reduced ability to form octamers because the band at 340 kDa was barely detectable (Fig. 4*A*, *upper panel*). The other bands given by C47S/C49S showed the same electrophoretic mobility as those from single mutants C47S and C49S. The bands at 172 and 128 kDa appeared more intense. One additional signal was faintly detected at 43 kDa, corresponding to PTX3 monomers. These results thus indicated that Cys^{47} and Cys^{49} are involved in PTX3 multimer formation.

We extended our investigation to Cys^{103} and observed that the single mutant C103S gave a band pattern shifted toward lower order oligomers as compared with those from wt PTX3 and C47S/C49S mutants. Similarly to C47S/C49S, C103S exhibited a band at 43 kDa and a low intensity signal at 340 kDa (Fig. 4*A*, *upper panel*). Additional bands were found at 260, 240, 200, and 190 kDa, which did not run at the same positions as any of those described above. Moreover the diffuse band at 172 kDa split in two distinct signals at 180 and 160 kDa. The C103S electrophoresis profile indicates that mutants lacking Cys^{103}-Cys^{103} interchain disulfide bonds form oligomers with electrophoretic properties different from those exhibited by wt PTX3 and C47S/C49S. This evidence is consistent with mass spectrometry data reporting Cys^{103} as engaged in symmetric inter-

chain disulfide bonds and confirmed a role for this residue in PTX3 covalent oligomerization.

The triple mutant C47S/C49S/C103S resolved as two major bands, an upper signal at 86 kDa and a lower signal at 43 kDa, representing PTX3 dimers and monomers, respectively (Fig. 4*B*, *upper panel*). Although definitely confirming the involvement of the N-terminal cysteines (Cys^{47}, Cys^{49}, and Cys^{103}) in PTX3 multimerization, these findings demonstrate that disulfide bonds formed by these residues are required to sustain the protein assembly into tetramers. In fact, the triple mutant C47S/C49S/C103S did not exhibit any significant signal above 86 kDa. Given the structural redundancy of Cys^{47} and Cys^{49} as described above, it follows that Cys^{103}-Cys^{103} disulfide bonds must join PTX3 subunits complementary to those bound through Cys^{47} and Cys^{49}. Furthermore the appearance of a dimer band at 86 kDa points to the presence of additional intersubunit disulfide bonds at the level of the PTX3 C-terminal domain. Our MS results showed that cysteine residues at proximal positions 317 and 318 formed both intra- and interdisulfide bonds. Therefore they were further analyzed by mutagenesis where the C317S/C318S double mutant gave two bands on SDS-PAGE at 172 and 86 kDa consistent with PTX3 tetramers and dimers, respectively (Fig. 4*B*, *upper panel*). The absence of bands at molecular mass higher than 172 kDa gives compelling evidence that Cys^{47}, Cys^{49}, and Cys^{103} provide the covalent framework for the assembly of PTX3 subunits into tetramers and indicates that the two interchain bonds formed by Cys^{317} and Cys^{318} link tetramer pairs into octamers. The quintuple mutant C47S/C49S/C103S/C317S/C318S was resolved into a cluster of bands around 43 kDa (Fig. 4*B*, *upper panel*), thus allowing the conclusion that this set of cysteines is necessary and sufficient for protein covalent oligomerization.

As expected, a 43-kDa band was detected upon reduction with DTT (Fig. 4, *A* and *B*, *lower panels*). A minor signal at 40 kDa was also observed that may result from oligosaccharide degradation (in particular the partial loss of terminal sialic acid residues) under the experimental conditions applied. Of note, the monomer band intensity appeared comparable among the different mutant species, thus indicating that the quantification by enzyme-linked immunosorbent assay was reliable.

A Model for PTX3 Assembly—A schematic map of the PTX3 interchain disulfide bond network is shown in Fig. 5. As described above, we demonstrated that PTX3 is predominantly organized into covalent octamers, so the protein is here represented as composed of eight subunits. Pairs of subunits are joined together by disulfide bonds involving Cys^{47} and Cys^{48}. The resulting dimers are then assembled into tetramers through covalent linkages provided by Cys^{103}. MS analysis revealed Cys^{317} and Cys^{318} to form both intra- and interchain disulfide bonds. Site-directed mutagenesis confirmed their involvement in intersubunit bridges. Accordingly in our model both intra- and interchain disulfide bonds were drawn at sites of Cys^{317} and Cys^{318}. We could not establish whether Cys^{317} and Cys^{318} are engaged in symmetric or asymmetric disulfide bonds. Nevertheless symmetric bonds are drawn in our model for simplicity. Because both mutants C103S and C47S/C49S exhibited higher oligomers than tetramers (Fig. 4*A*, *upper panel*), we hypothesized that six $Cys^{317/318}$-$Cys^{317/318}$ interchain and two Cys^{317}-Cys^{318} intrachain disulfide bonds occur in the molecule. Thus it is possible for PTX3 to form oligomers up to octamers when Cys^{103}-Cys^{103}, Cys^{47}-Cy^{47}, and Cys^{49}-Cys^{49} are missing. However, as $Cys^{47/49}$ and Cys^{103} mutagenesis greatly reduced the octamer band intensity while increasing the strength of the hexamer, tetramer, and dimer signals, it is likely that the protein assembles into octamers containing not only six but also four or two $Cys^{317/318}$-$Cys^{317/318}$ interchain disulfide bonds (see supplemental Fig. S3).

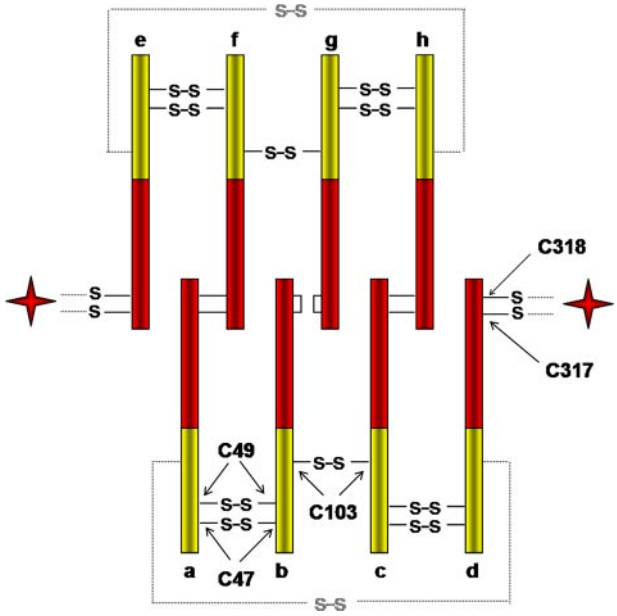

FIGURE 5. **Schematic diagram of PTX3 covalent assembly.** A schematic map showing the disulfide bond network stabilizing PTX3 multimerization is shown. PTX3 subunits are drawn as *bars* and labeled by a *letter code* (protomers *a*–*h*). The protein N- and C-terminal domains are highlighted in *yellow* and *red*, respectively. *Arrows* point to approximate positions of interchain disulfide bonds. The intrachain Cys^{317}-Cys^{318} bond is also shown (*i.e.* on subunits *b* and *g*). Two *red stars* on the opposite sides of the model indicate that subunits d and e are bound through two disulfide bonds involving Cys^{317} and Cys^{318}.

Analysis of PTX3 Mutants by Native PAGE—To further assess the contribution provided by disulfide bonds to protein oligomerization, we submitted PTX3 Cys to Ser mutants to WB analysis under native conditions. Data from gels were then used to graph Ferguson plots as described above. As apparent in Fig. 6, showing the gel at 5.5%, band patterns exhibited by wt PTX3 and C47S/C49S/C103S triple mutant were essentially identical (Fig. 6*A*, *lanes 1* and *2*). The major band in C47S/C49S/C103S electrophoretic profile migrated at an apparent molecular mass of 336 kDa, corresponding to PTX3 octamers. This indicates that PTX3 protomers are able to self-assemble into high order oligomers regardless of the interchain disulfide bonds formed by the N-terminal domain cysteine residues.

The double mutant C317S/C318S showed a main signal at 170 kDa, consistent with PTX3 tetramers, and a minor band at 336 kDa (Fig. 6*A*, *lane 3*), demonstrating that, despite a clear impairment in PTX3 octameric assembly, the protein retains the ability to form tetramers when the two linkages established by Cys^{317} and Cys^{318} are missing. Therefore, these disulfide bonds appear to play an essential role in covalent dimerization of PTX3 tetramers to give octamers.

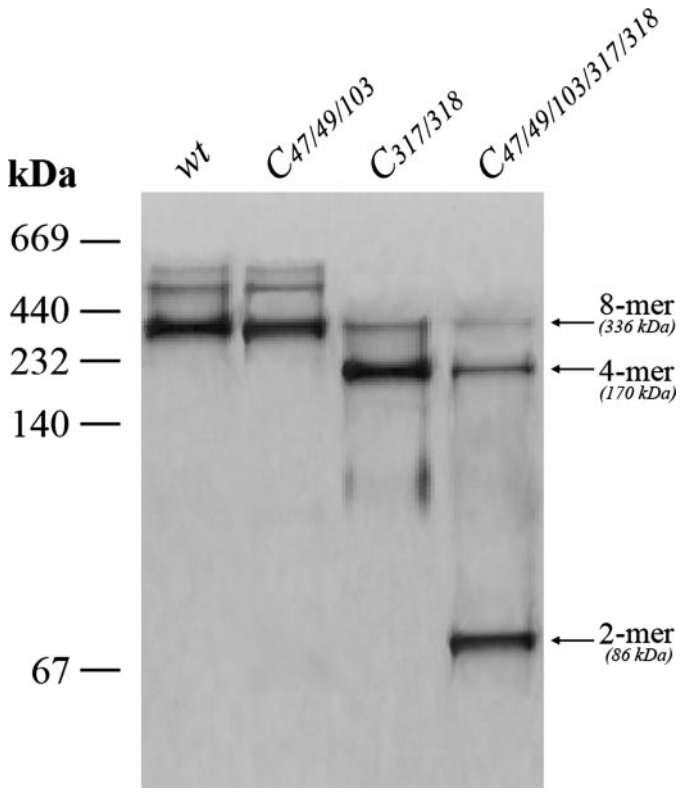

FIGURE 6. **WB analysis of PTX3 Cys to Ser mutants under non-denaturing conditions.** wt PTX3 and C47S/C49S/C103S ($C_{47/49/103}$), C317S/C318S ($C_{317/318}$), and C47S/C49S/C103S/C317S/C318S ($C_{47/49/103/317/318}$) mutants were resolved on native gels and detected by immunoblot as described in Fig. 1. Electrophoresis mobility data were then submitted to Ferguson plot analysis (see "Experimental Procedures"). Only the 5.5% gel is shown. The molecular masses of thyroglobulin (669 kDa), ferritin (440 kDa), catalase (232 kDa), lactate dehydrogenase (140 kDa), and albumin (67 kDa) were used as calibrants and are shown on the *left-hand side*. Molecular mass and oligomeric status of resolved bands, as measured by Ferguson plot, are shown on the *right-hand side*.

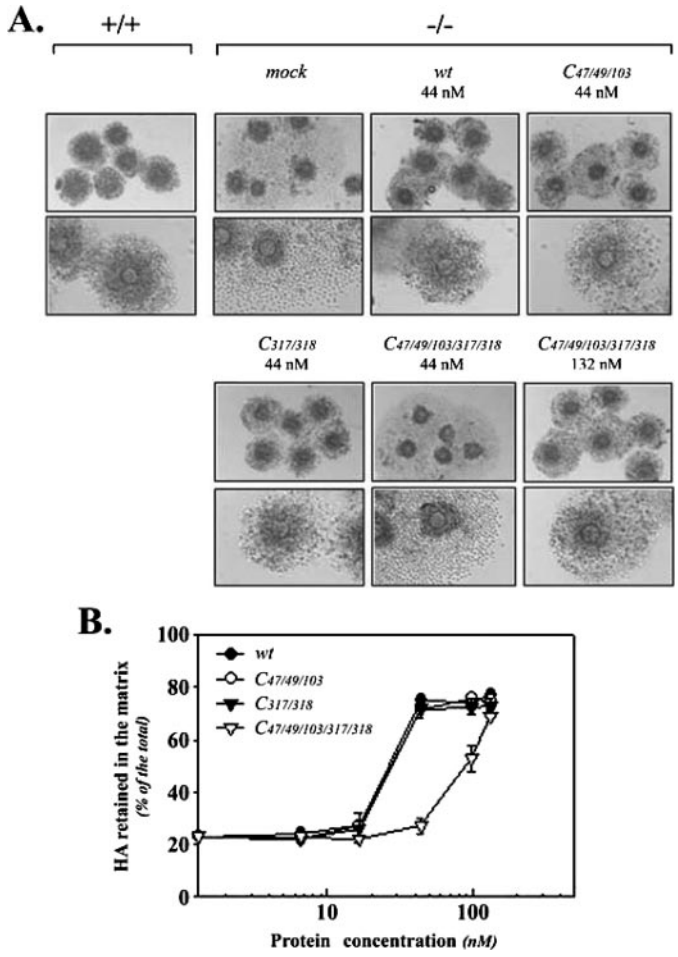

FIGURE 7. **PTX3 Cys to Ser mutants rescue activity in defective COCs.** Wild type (+/+) and *Ptx3*-null (−/−) COCs were cultured for 16 h with 100 ng/ml follicle-stimulating hormone plus 1% fetal calf serum in the absence or presence of wt PTX3 or PTX3 Cys to Ser mutants at different concentrations. *A*, micrographs showing $Ptx3^{+/+}$ and $Ptx3^{-/-}$ COC morphology at the end of culture. *B*, HA titers in the matrix surrounding oocytes were measured and plotted *versus* protein concentration. Data, expressed as percentage of total HA, are representative of three independent experiments (mean ± S.D.). C47S/C49S/C103S, C317S/C318S, and C47S/C49S/C103S/C317S/C318S mutants are indicated as $C_{47/49/103}$, $C_{317/318}$, and $C_{47/49/103/317/318}$, respectively.

The quintuple mutant C47S/C49S/C103S/C317S/C318S migrated on native gels mainly as a dimer (Fig. 6*A*, *lane 4*), suggesting that the N-terminal Cys^{47}, Cys^{49}, and Cys^{103} and the C-terminal Cys^{317} and Cys^{318} provide interdependent contributions to the stabilization of protein oligomers. Moreover the appearance of minor tetramer and octamer bands indicates a residual PTX3 self-assembly ability even in the absence of the entire set of interchain disulfide bonds. Densitometry analysis indicated relative intensities of about 70, 20, and 10% for dimer, tetramer, and octamer bands, respectively, of the quintuple mutant C47S/C49S/C103S/C317S/C318S (data not shown).

Rescue of Defective Cumulus Expansion by PTX3 Mutants—To investigate the effect of PTX3 oligomeric status on the protein biological activity, C47S/C49S/C103S, C317S/C318S, and C47S/C49S/C103S/C317S/C318S mutants were assayed for their ability to rescue normal phenotype in COCs from *Ptx3*-null mice. It has been shown that COCs from *Ptx3*-null mice, stimulated *in vitro* for 16 h with hormones, become disorganized as a consequence of a defective HA organization into the viscoelastic matrix holding together cumulus cells and oocyte (8). This phenomenon can be reverted by supplementing $Ptx3^{-/-}$ COC cultures with recombinant PTX3 (9). Recent findings suggest that PTX3 stabilization of cumulus matrix might depend on the protein multimeric arrangement (9, 16). Thus, we evaluated $Ptx3^{-/-}$ COC morphology and HA distribution between medium and matrix after 16-h hormone treatment in the presence of increasing concentrations of different PTX3 mutants and wt protein. C47S/C49S/C103S and C317S/C318S, forming mainly octamers and tetramers, respectively, showed the same potency as the wt PTX3, allowing maximum HA retention within the matrix and COC integrity at the minimum applied dose of 44 nM (Fig. 7, *A* and *B*). Conversely the quintuple mutant C47S/C49S/C103S/C317S/C318S, forming mainly dimers, proved to be about 3 times less active because the normal phenotype of $Ptx3^{-/-}$ COCs was rescued only at the dose of 132 nM. This activity tightly correlates with the overall proportion of tetramers and octamers (compared with dimers) in the quintuple mutant (which make up 30% of the total protein; see above). These results suggest that the minimum oligomeric status required for PTX3 to exert its role in COC matrix organization is the tetramer.

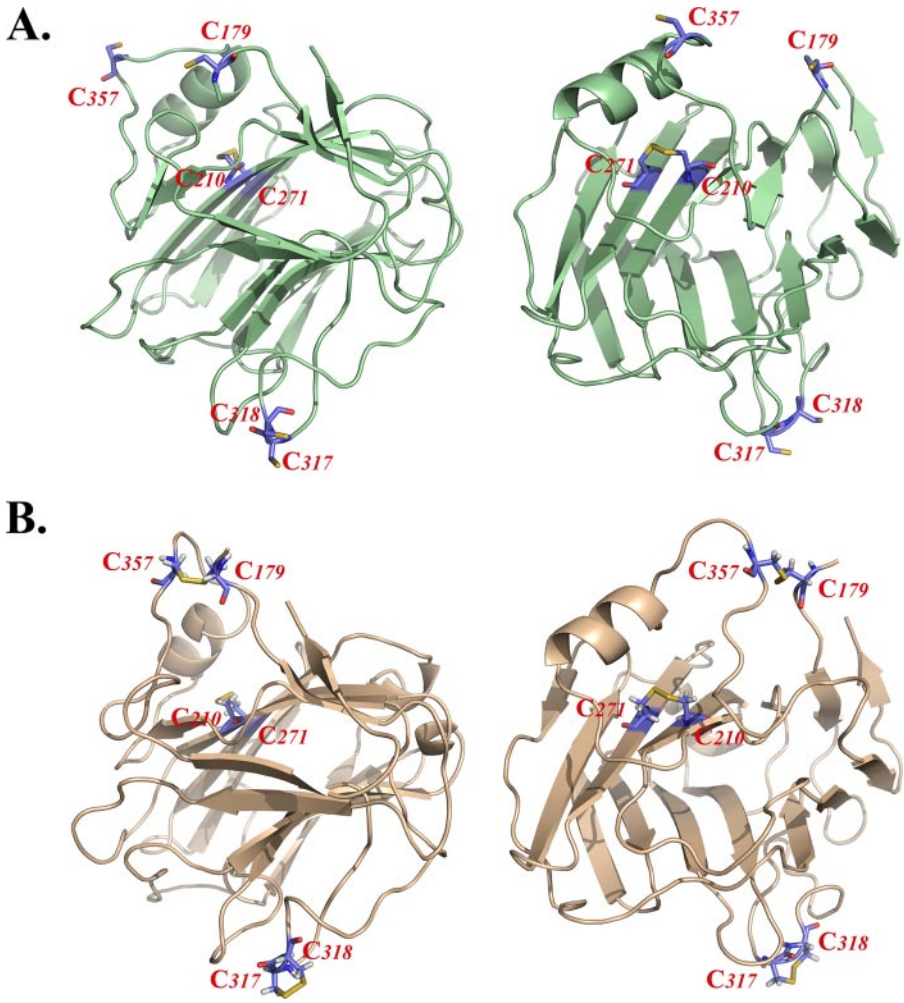

FIGURE 8. **A new model for PTX3 C-terminal domain.** *A*, three-dimensional model of PTX3 C-terminal domain based on CRP crystal structure (Protein Data Bank code 1b09). *B*, Cys^{179}-Cys^{357} and Cys^{317}-Cys^{318} intrachain disulfide bonds were integrated into the model shown in *A*, and the structure was optimized by molecular dynamics. Shown is the resulting refined model. Two orthogonal aligned views of both models are shown in *A* and *B*. *Ribbons* are representative of secondary structure elements. Cys^{179}, Cys^{210}, Cys^{271}, Cys^{317}, Cys^{318}, and Cys^{357} residues, found by mass spectrometry to form disulfide bonds, are reported as *colored sticks* and labeled in *red*.

Three-dimensional Model of PTX3 C-terminal Domain—We previously built by homology modeling a three-dimensional model of the PTX3 C-terminal domain using as a template the crystallographic structure of CRP (Protein Data Bank code 1b09) (24) (Fig. 8*A*). This model contains a disulfide bond, involving Cys^{210} and Cys^{271}, that is highly conserved among pentraxins (21, 22). Both mass spectrometry and site-directed mutagenesis data shown here indicated that also Cys^{179} and Cys^{357} form an intrachain disulfide bond. According to our model, Cys^{179} and Cys^{357} are in loop regions facing each other that show the flexibility required to bring the two residues close enough to form a disulfide bond, consistent with our experimental evidence. The Cys^{179}-Cys^{357} disulfide bond was integrated as a new structural constraint in a refined model of the PTX3 C-terminal domain (Fig. 8*B*). In the new model the Cys^{179}-Cys^{357} disulfide bond links the N- and C-terminal ends of the PTX3 C-terminal domain, thus limiting the flexibility of these regions. Moreover we report Cys^{317} and Cys^{318} as engaged in both intra- and interchain disulfide bonds. These two cysteines are localized in an exposed loop, which is likely to represent part of the PTX3 regions at the protomer interface.

DISCUSSION

In this study we have provided new insights on PTX3 oligomeric structure and have begun to address the role that it plays in PTX3 function. The network of PTX3 disulfide bonds was characterized by two complementary approaches: mass spectrometry and site-directed mutagenesis. Mass spectrometry identified cysteine residues involved in disulfide bond formation, whereas PAGE analysis of PTX3 Cys to Ser mutants allowed the determination of how disulfide bonds are distributed within and between the protein subunits.

Previous studies showed that PTX3 is eluted in gel filtration chromatography with an apparent molecular mass of ~900 kDa. It was concluded that this corresponds to a 20-mer, whereas native PAGE revealed the protein to predominantly form multimers of ~440 kDa thought to correspond to 10-mers (23). It is known that for accurate determination of molecular weight by size exclusion chromatography the protein of interest must have the same relationship between molecular weight and molecular size and shape as the calibration standards (46), which are usually globular. The PTX3 molecule might not have a globular shape. If so, it would show a higher hydrodynamic radius than the one expected for a globular protein with comparable molecular weight, which might account for the molecular mass of ~900 kDa measured under size exclusion chromatography conditions. An additional complication might come from PTX3 glycosylation (24) because the determination of the molecular weight for glycoproteins by size exclusion chromatography may not correlate well to the calibration curves plotted for globular non-glycosylated proteins (46). Furthermore it is well established that protein mobility on native gels is a function of its charge, shape, and mass so information on protein molecular weight inferred from single native gels might sometimes be misleading (47). To overcome these limitations we determined the molecular weight of PTX3 by Ferguson plot on native PAGE, which offers the distinctive advantage of providing charge-independent molecular weight measurements (40). We reported a molecular mass of 336 kDa for the major species on native gels; this is consistent with that of a PTX3 octamer. SDS-PAGE analysis

confirmed this view because a major band at an apparent molecular mass of 340 kDa was observed on Tris acetate gradient gels. During new investigations on PTX3 quaternary structure, we have recently exploited multiangle laser light scattering to determine the molecular weight of PTX3 under non-denaturing gel filtration conditions. Measurements performed by multiangle laser light scattering were consistent with data from native and denaturing PAGE.[5] Taken together, these results indicate that PTX3 subunits mainly assemble into covalently linked octamers. Although SAP from *Limulus polyphemus* hemolymph has been described to fold into a doubly stacked octameric ring (48), the octameric assembly here described for human PTX3 appears to be unique among the vertebrates pentraxins (21, 22, 33).

Western blotting revealed minor bands that can be attributed to lower order oligomers (hexamers, pentamers, tetramers, and dimers). Faint bands were detected on native gels at 422, 514, and 700 kDa (corresponding to PTX3 10-mers, 12-mers, and 16-mers, respectively); thus they may be derived from the non-covalent association of octamers and lower order oligomers, consistent with the tendency of the protein to self-assemble into higher order oligomers (23).

Here we report that the cysteine residues located in the N-terminal domain of PTX3 form disulfide bonds arranging the protein into tetramers. In this regard, Cys^{47}-Cys^{47} and Cys^{49}-Cys^{49} bonds stabilize protein dimers, pairs of which are then linked through Cys^{103}-Cys^{103} bonds. The resulting tetramers are finally assembled into octamers by disulfide bridges involving Cys^{317} and Cys^{318} (Fig. 5). In principle two $Cys^{317/318}$-$Cys^{317/318}$ interchain bonds (Cys^{317}-Cys^{318} and Cys^{318}-Cys^{317} or Cys^{317}-Cys^{317} and Cys^{318}-Cys^{318}) between two distinct PTX3 tetramers might be sufficient to organize PTX3 into octamers. However, as octameric species were still observed in the electrophoretic profile of mutants C103S and C47S/C49S and the band intensity of hexamers, tetramers, and dimers increased following both $Cys^{47/49}$ and Cys^{103} mutagenesis (Fig. 4, *upper panel*), it is likely that the functional protein forms octamers containing up to six $Cys^{317/318}$-$Cys^{317/318}$ interchain disulfide bonds (supplemental Fig. S3). Although we cannot rule out the formation of $Cys^{317/318}$-$Cys^{317/318}$ interchain bonds within tetramers, this seems unlikely because these cysteines were described to mediate the covalent association of tetramers into octamers and as such are probably located at the interface between C-terminal domains on distinct tetramers. $Cys^{317/318}$-$Cys^{317/318}$ interchain disulfides were described to involve both Cys^{317} and Cys^{318} residues. Whether these two disulfide bonds are symmetric (Cys^{317}-Cys^{317} and Cys^{318}-Cys^{318}) or asymmetric (Cys^{317}-Cys^{318} and Cys^{318}-Cys^{317}) remains unsolved. Mass spectrometry showed that Cys^{317} and Cys^{318} form intra- as well as interchain disulfide bonds. Although Cys^{317} and Cys^{318} are not conserved among pentraxins, two adjacent cysteines were identified at equivalent positions in the C-terminal end of rat CRP (*i.e.* amino acids 208 and 209) (49). These cysteines were found to be engaged either in inter- or intrachain disulfide bonds analogous to what we described here for PTX3 Cys^{317} and Cys^{318} (49).

A model of the PTX3 C-terminal domain was constructed by homology modeling using the crystallographic structure of CRP (Fig. 8*A*). In this model, the Cys^{210}-Cys^{271} disulfide bond stabilizes two antiparallel β-sheets organized in a typical β-jelly roll topology, equivalent to the structural role these conserved residues perform in the classical pentraxins CRP and SAP (21, 22). Our mass spectrometry data indicated Cys^{179} and Cys^{357} to form a disulfide bond too. Results from Cys to Ser site-directed mutagenesis allowed us to infer this bond to be of the intrachain type. In the C-terminal domain three-dimensional model, Cys^{179} and Cys^{357} were found positioned close enough to support a covalent linkage. Experimental data thus provided evidence as to the reliability of the proposed model. We then elaborated a refined structure of the PTX3 C-terminal domain by integrating as structural constraints the newly identified Cys^{179}-Cys^{357} and Cys^{317}-Cys^{318} intrachain bonds. The overall domain fold is essentially unaffected by the new bonds (Fig. 8*B*). The Cys^{179}-Cys^{357} disulfide links the N-terminal end to the C-terminal end of the pentraxin domain thus limiting the flexibility of these two regions. The Cys^{317}-Cys^{318} intrachain bond is localized in an exposed loop, which is likely to represent part of the interface between protomer subunits.

We described the disulfide bond network established by the N-terminal cysteines as essential for PTX3 oligomerization. Interestingly the N-terminal domain of other long pentraxins such as the neuronal pentraxins NP1 (33) and NP2 (34) and some collectins, a family of proteins that share with PTX3 the ability to recognize microorganisms and enhance their engulfment by phagocytes (50, 51), includes cysteine residues with a similar structural role, although these domains do not share sequence homology.

The N-terminal region of PTX3 is not related to any known protein sequence; nevertheless it has been predicted to be composed of four α-helices, which are likely to adopt a coiled coil conformation (52). Coiled coils are also found in the N-terminal domain of NP1 (33) and NP2 (34) as well as in the neck region of collectins (50, 51). This structural motif is mainly found in modular proteins and exerts a key function in protein oligomerization through non-covalent interactions (53). In agreement with these structural features, our data from native PAGE analysis of PTX3 Cys to Ser mutants provided evidence that the protein N-terminal domain mainly contains the structural determinants responsible for PTX3 oligomerization. Indeed although C47S/C49S/C103S was resolved under denaturing conditions as a dimer, this mutant migrated on native gels mainly as an octamer, exhibiting a self-assembly ability even when the entire set of N-terminal disulfide bonds was missing. In contrast, the association between the C-terminal domains mostly relied on the $Cys^{317/318}$-$Cys^{317/318}$ interchain disulfide bonds to form. C317S/C318S was, indeed, only partially able to assemble into octamers (Fig. 6).

Previous studies support the notion that PTX3 exerts its structural role within the cumulus matrix as a multimeric protein (9, 16). A model for the role of PTX3 in cumulus matrix assembly has been proposed where heavy chains, transferred from inter-α-inhibitor to HA by the catalytic activity of TSG-6,

[5] A. Inforzato, T. A. Jowitt, D. A. Holmes, B. Bottazzi, G. Salvatori, A. Mantovani, and A. J. Day, manuscript in preparation.

bind distinct protomers of multimeric PTX3, leading to HA cross-linking (16). Here we showed that PTX3 multimeric organization is essential to the protein activity in cumulus matrix. Furthermore we described the tetramer as the lowest PTX3 oligomer still retaining full functionality in cumulus matrix assembly and stabilization. The mutant C317S/C318S, exhibiting mainly a tetrameric assembly under native PAGE conditions, was indeed as effective as the wt protein in restoring normal cumulus expansion *ex vivo*. Analogous effectiveness on cumuli isolated from *Ptx3*$^{-/-}$ mice was observed with C47S/C49S/C103S, which preserved the octameric structure. We could not test the functionality of PTX3 monomers in cumuli as the mutant C47S/C49S/C103S/C317S/C318S lacking the entire network of interchain disulfide bonds predominantly formed dimers. On native gels about 70% of C47S/C49S/C103S/C317S/C318S was dimer, 20% was tetramer, and the remaining 10% was octamer; these oligomeric states, which result from the non-covalent association between PTX3 monomers, are presumably in equilibrium. The correlation between the reduction in this mutant activity (2–3 times less effective than the wt protein) and the fraction of the dimeric species (about ⅔ of the total) suggest that the residual rescue activity is derived from the tetramers/octamers present in the sample.

The heavy chain-binding site has been localized in the PTX3 N-terminal domain (16). Accordingly a recombinant form of this domain allows normal *in vitro* expansion of *Ptx3*$^{-/-}$ COCs, thus mimicking the function of the full-length protein (16). It has been reported that the isolated PTX3 N-terminal domain assembles into disulfide bond-stabilized oligomers (9, 16). Here we describe that the N-terminal domains of the full-length PTX3 are composed of two structurally independent tetramers by the three symmetric disulfide bonds Cys^{47}-Cys^{47}, Cys^{49}-Cys^{49}, and Cys^{103}-Cys^{103}.

In previous studies it has been proposed that PTX3 acts as a node in the cumulus matrix for example by establishing direct multivalent interaction with either the hyaladherin TSG-6 (9) or the serum protein inter-α-inhibitor (16). Here we provide evidence for the nodal activity of PTX3 in that our data indicate that the multimeric organization of PTX3 is essential to its function with the PTX3 tetramer as the functional molecular unit required for cumulus matrix organization. Further studies are in progress to determine whether the degree of oligomerization may influence other biological functions of PTX3, such as complement activation, angiogenesis, and protection against opportunistic pathogens.

Acknowledgments—We thank the Biomolecular Analysis Facility, Faculty of Life Sciences, University of Manchester (supported by the Wellcome Trust) and Dr. Domenico Mastroianni from Tecnogen S.p.A. for the valuable help in performing the mass spectrometry analyses.

REFERENCES

1. Breviario, F., d'Aniello, E. M., Golay, J., Peri, G., Bottazzi, B., Bairoch, A., Saccone, S., Marzella, R., Predazzi, V., and Rocchi, M. (1992) *J. Biol. Chem.* **267,** 22190–22197
2. Lee, G. W., Lee, T. H., and Vilcek, J. (1993) *J. Immunol.* **150,** 1804–1812
3. Alles, V. V., Bottazzi, B., Peri, G., Golay, J., Introna, M., and Mantovani, A. (1994) *Blood* **84,** 3483–3493
4. Doni, A., Michela, M., Bottazzi, B., Peri, G., Valentino, S., Polentarutti, N., Garlanda, C., and Mantovani, A. (2006) *J. Leukoc. Biol.* **79,** 797–802
5. Vouret-Craviari, V., Matteucci, C., Peri, G., Poli, G., Introna, M., and Mantovani, A. (1997) *Infect. Immun.* **65,** 1345–1350
6. Garlanda, C., Hirsch, E., Bozza, S., Salustri, A., De Acetis, M., Nota, R., Maccagno, A., Riva, F., Bottazzi, B., Peri, G., Doni, A., Vago, L., Botto, M., De Santis, R., Carminati, P., Siracusa, G., Altruda, F., Vecchi, A., Romani, L., and Mantovani, A. (2002) *Nature* **420,** 182–186
7. Gaziano, R., Bozza, S., Bellocchio, S., Perruccio, K., Montagnoli, C., Pitzurra, L., Salvatori, G., De Santis, R., Carminati, P., Mantovani, A., and Romani, L. (2004) *Antimicrob. Agents Chemother.* **48,** 4414–4421
8. Varani, S., Elvin, J. A., Yan, C., DeMayo, J., DeMayo, F. J., Horton, H. F., Byrne, M. C., and Matzuk, M. M. (2002) *Mol. Endocrinol.* **16,** 1154–1167
9. Salustri, A., Garlanda, C., Hirsch, E., De Acetis, M., Maccagno, A., Bottazzi, B., Doni, A., Bastone, A., Mantovani, G., Beck Peccoz, P., Salvatori, G., Mahoney, D. J., Day, A. J., Siracusa, G., Romani, L., and Mantovani, A. (2004) *Development* **131,** 1577–1586
10. Nauta, A. J., Bottazzi, B., Mantovani, A., Salvatori, G., Kishore, U., Schwaeble, W. J., Gingras, A. R., Tzima, S., Vivanco, F., Egido, J., Tijsma, O., Hack, E. C., Daha, M. R., and Roos, A. (2003) *Eur. J. Immunol.* **33,** 465–473
11. Roumenina, L. T., Ruseva, M. M., Zlatarova, A., Ghai, R., Kolev, M., Olova, N., Gadjeva, M., Agrawal, A., Bottazzi, B., Mantovani, A., Reid, K. B., Kishore, U., and Kojouharova, M. S. (2006) *Biochemistry* **45,** 4093–4104
12. Rusnati, M., Camozzi, M., Moroni, E., Bottazzi, B., Peri, G., Indraccolo, S., Amadori, A., Mantovani, A., and Presta, M. (2004) *Blood* **104,** 92–99
13. Camozzi, M., Zacchigna, S., Rusnati, M., Coltrini, D., Ramirez-Correa, G., Bottazzi, B., Mantovani, A., Giacca, M., and Presta, M. (2005) *Arterioscler. Thromb. Vasc. Biol.* **25,** 1837–1842
14. Milner, C. M., and Day, A. J. (2003) *J. Cell Sci.* **116,** 1863–1873
15. Day, A. J., and de la Motte, C. A. (2005) *Trends Immunol.* **26,** 637–643
16. Scarchilli, L., Camaioni, A., Bottazzi, B., Negri, V., Doni, A., Deban, L., Bastone, A., Salvatori, G., Mantovani, A., Siracusa, G., and Salustri, A. (2007) *J. Biol. Chem.* **282,** 30161–30170
17. Rovere, P., Peri, G., Fazzini, F., Bottazzi, B., Doni, A., Bondanza, A., Zimmermann, V. S., Garlanda, C., Fascio, U., Sabbadini, M. G., Rugarli, C., Mantovani, A., and Manfredi, A. A. (2000) *Blood* **96,** 4300–4306
18. van Rossum, A. P., Fazzini, F., Limburg, P. C., Manfredi, A. A., Rovere-Querini, P., Mantovani, A., and Kallenberg, C. G. (2004) *Arthritis Rheum.* **50,** 2667–2674
19. Baruah, P., Dumitriu, I. E., Peri, G., Russo, V., Mantovani, A., Manfredi, A. A., and Rovere-Querini, P. (2006) *J. Leukoc. Biol.* **80,** 87–95
20. Baruah, P., Propato, A., Dumitriu, I. E., Rovere-Querini, P., Russo, V., Fontana, R., Accapezzato, D., Peri, G., Mantovani, A., Barnaba, V., and Manfredi, A. A. (2006) *Blood* **107,** 151–158
21. Pepys, M. B., and Baltz, M. L. (1983) *Adv. Immunol.* **34,** 141–212
22. Goodman, A. R., Cardozo, T., Abagyan, R., Altmeyer, A., Wisniewski, H. G., and Vilcek, J. (1996) *Cytokine Growth Factor Rev.* **7,** 191–202
23. Bottazzi, B., Vouret-Craviari, V., Bastone, A., De Gioia, L., Matteucci, C., Peri, G., Spreafico, F., Pausa, M., D'Ettorre, C., Gianazza, E., Tagliabue, A., Salmona, M., Tedesco, F., Introna, M., and Mantovani, A. (1997) *J. Biol. Chem.* **272,** 32817–32823
24. Inforzato, A., Peri, G., Doni, A., Garlanda, C., Mantovani, A., Bastone, A., Carpentieri, A., Amoresano, A., Pucci, P., Roos, A., Daha, M. R., Vincenti, S., Gallo, G., Carminati, P., De Santis, R., and Salvatori, G. (2006) *Biochemistry* **45,** 11540–11551
25. Kaplan, M. H., and Volanakis, J. E. (1974) *J. Immunol.* **112,** 2135–2147
26. Agrawal, A., Scrive, A. K., Greenhough, T. J., and Volanakis, J. E. (2001) *J. Immunol.* **166,** 3998–4004
27. Bristol, C. L., and Boackle, R. J. (1986) *Mol. Immunol.* **23,** 1045–1052
28. Ying, S. C., Gewurz, A. T., Jiang, H., and Gewurz, H. (1993) *J. Immunol.* **150,** 169–176
29. Camozzi, M., Rusnati, M., Bugatti, A., Bottazzi, B., Mantovani, A., Bastone, A., Inforzato, A., Vincenti, S., Bracci, L., Mastroianni, D., and Presta, M. (2006) *J. Biol. Chem.* **281,** 22605–22613
30. Khreiss, T., József, L., Potempa, L. A., and Filep, J. G. (2004) *Circulation* **110,** 2713–2720

31. Zouki, C., Haas, B., Chan, J. S., Potempa, L. A., and Filep, J. G. (2001) *J. Immunol.* **167,** 5355–5361
32. Bíró, A., Rovó, Z., Papp, D., Cervenak, L., Varga, L., Füst, G., Thielens, N. M., Arlaud, G. J., and Prohászka, Z. (2007) *Immunology* **121,** 40–50
33. Omeis, I. A., Hsu, Y. C., and Perin, M. S. (1996) *Genomics* **36,** 543–545
34. Hsu, Y. C., and Perin, M. S. (1995) *Genomics* **28,** 220–227
35. Xu, D., Hopf, C., Reddy, R., Cho, R. W., Guo, L., Lanahan, A., Petralia, R. S., Wenthold, R. J., O'Brien, R. J., and Worley, P. (2003) *Neuron* **39,** 513–528
36. Emsley, J., White, H. E., O'Hara, B. P., Oliva, G., Srinivasan, N., Tickle, I. J., Blundell, T. L., Pepys, M. B., and Wood, S. P. (1994) *Nature* **367,** 338–345
37. Thompson, D., Pepys, M. B., and Wood, S. P. (1999) *Struct. Fold. Des.* **7,** 169–177
38. Introna, M., Alles, V. V., Castellano, M., Picardi, G., De Gioia, L., Bottazzi, B., Peri, G., Breviario, F., Salmona, M., De Gregorio, L., Dragani, T. A., Srinivasan, N., Blundell, T. L., Hamilton, T. A., and Mantovani, A. (1996) *Blood* **87,** 1862–1872
39. Rivieccio, V., Esposito, A., Bellofiore, P., Palladino, P., Sassano, M., Colombo, M., and Verdoliva, A. (2007) *Protein Expr. Purif.* **51,** 49–58
40. Butterman, M., Tietz, D., Orbán, L., and Chrambach, A. (1988) *Electrophoresis* **9,** 293–298
41. Ho, S. N., Hunt, H. D., Horton, R. M., Pullen, J. K., and Pease, L. R. (1989) *Gene* (*Amst.*) **77,** 51–59
42. Mohamadi, F., Richards, N. G. J., Guida, W. C., Liskamp, R., Lipton, M., Caufield, C., Chang, G., Hendrickson, T., and Still, W. C. (1990) *J. Comput. Chem.* **11,** 440–467
43. Laskowsky, R. A., MacArthur, M. W., Moss, D. S., and Thornton, J. M. (1993) *J. Appl. Crystallogr.* **26,** 283–291
44. Ellman, G. L. (1959) *Arch. Biochem. Biophys.* **82,** 70–77
45. Robyt, J. F., Ackerman, R. J., and Chittenden, C. G. (1971) *Arch. Biochem. Biophys.* **147,** 262–269
46. Andrews, P. (1970) in *Methods of Biochemical Analysis* (Glick, D. ed) pp. 113–176, Interscience Publishers, New York
47. Rodbard, D., and Chrambach, A. (1970) *Proc. Natl. Acad. Sci. U. S. A.* **65,** 970–977
48. Shrive, A. K., Metcalfe, A. M., Cartwright, J. R., and Greenhough, T. J. (1999) *J. Mol. Biol.* **290,** 997–1008
49. Rassouli, M., Sambasivam, H., Azadi, P., Dell, A., Morris, H. R., Nagpurkar, A., Mookerjea, S., and Murray, R. K. (1992) *J. Biol. Chem.* **267,** 2947–2954
50. Kishore, U., and Reid, K. B. (2001) *Results Probl. Cell Differ.* **33,** 225–248
51. McCormack, F. X., and Whitsett, J. A. (2002) *J. Clin. Investig.* **109,** 707–712
52. Presta, M., Camozzi, M., Salvatori, G., and Rusnati, M. (2007) *J. Cell. Mol. Med.* **11,** 723–738
53. Lupas, A. N., and Gruber, M. (2005) *Adv. Protein Chem.* **70,** 37–78

Structural Characterization of PTX3 Disulfide Bond Network and Its Multimeric Status in Cumulus Matrix Organization

Antonio Inforzato, Vincenzo Rivieccio, Antonio P. Morreale, Antonio Bastone, Antonietta Salustri, Laura Scarchilli, Antonio Verdoliva, Silvia Vincenti, Grazia Gallo, Caterina Chiapparino, Lucrezia Pacello, Eleonora Nucera, Ottaviano Serlupi-Crescenzi, Anthony J. Day, Barbara Bottazzi, Alberto Mantovani, Rita De Santis and Giovanni Salvatori

J. Biol. Chem. 2008, 283:10147-10161.
doi: 10.1074/jbc.M708535200 originally published online January 25, 2008
